Highly Efficient Deep-Blue Organic Light-Emitting Diodes Based on Pyreno[4,5-d]imidazole-Anthracene Isomers

Hui Liu,[a] Liangliang Kang,[b] Jinyu Li,[a] Futong Liu,[a] Xin He,[a] Shenghong Ren,[a] Xiangyang Tang,[a] Changli Lv,[b] and Ping Lu*,[a]

Contents

1 Experimental Section

1.1 General Information

All the reagents and solvents used for the synthesis were purchased from Aldrich and Acros companies and used without further purification. The synthesis procedure was presented in Scheme S1. The ^{1}H and ^{13}C NMR data were recorded on a Bruker AVANCE 500 spectrometer at 500 MHz and 125 MHz respectively, using tetramethylsilane (TMS) as the internal standard and DMSO-D_6 or $CDCl_3$ as solvent. The phase composition of evaporated film of samples was examined by X-ray diffraction (XRD, Rigaku D/MAX 2550) in the angular range of 2Θ = 10-60° with Cu

Ka radiation. The operating voltage and current were kept at 50 kV and 200 mA in an ambient environment. The infrared (IR) spectra in the range of 400-4000 cm^{-1} was acquired on a Fourier transform infrared spectrometer (Brucker, VERTEX 80V) with KBr as basement. The element contents of the compounds were characterized by a Flash EA 1112, CHNS-O elemental analysis instrument. The MALDI-TOF mass spectra were recorded by an AXIMA-CFRTM plus instrument. Thermal gravimetric analysis (TGA) was undertaken on a PerkinElmer thermal analysis system with a heating rate of 10 °C min^{-1}. Differential scanning calorimetry (DSC) analysis was carried out through a NETZSCH (DSC-204) instrument at 10 °C min^{-1} while flushing with nitrogen. UV-vis absorption spectra were recorded on a UV-3100 spectrophotometer. Fluorescence measurements were carried out with a RF-5301PC. The fluorescence lifetime was measured using FLS920 Spectrometer with a 375 nm picosecond pulsed light emitting diode excitation source (pulse with: 898.3 ps). The photoluminescence quantum yield (PLQY, Φ) is measured by integrating sphere.

1.2 Electrochemical Measurement

Cyclic voltammetry (CV) was performed with a BAS 100W Bioanalytical Systems, using a glass carbon disk (Φ = 3 mm) as the working electrode, a platinum wire as the auxiliary electrode with a porous ceramic wick, Ag/Ag^{+} as the reference electrode, standardized for the redox couple ferricinium/ferrocene. In each case, the anodic scan was performed in dichloromethane (DCM), while the cathodic scan was conducted in dry degassed DMF. All solutions were purged with nitrogen stream for 10 min before measurements. The procedure was performed at room temperature and a nitrogen atmosphere was maintained over the solution during measurements. The HOMO and LUMO energy levels of the materials versus the vacuum levels were calculated from the estimated onset potential of oxidation and reduction by assuming the absolute energy level of ferrocene was 4.8 eV below the vacuum level.

$$E_{HOMO} = -\ [\,4.8 + (E_{ox}^{onset} - E_{Fc/Fc+})\,]\ \text{eV} \qquad (1)$$

$$E_{LUMO} = -\ [\,4.8 + (E_{red}^{onset} - E'_{Fc/Fc+})\,]\ \text{eV} \quad (2)$$

$$E_g = (E_{LUMO} - E_{HOMO})\ \text{eV} \quad (3)$$

where 4.8 eV is the absolute energy level of Fc below vacuum, E_{ox}^{onset} and E_{red}^{onset} are the onset potentials of the materials obtained from positive and negative CV scans, respectively, and $E_{Fc/Fc+}$ and $E_{Fc/Fc+}'$ are half wave potentials of ferrocene redox couple obtained from positive and negative CV scans, respectively.

1.3 Device Fabrication

ITO-coated glass with a sheet resistance of 20 Ω square^{-1} was used as the substrate. Before device fabrication, the ITO glass substrates were cleaned with isopropyl alcohol and deionized water, dried in an oven at 120 °C, treated with UV-zone for 20 min, and finally transferred to a vacuum deposition system with the base pressure lower than 5×10^{-4} Pa for organic and metal deposition. The devices were fabricated by evaporating organic layers with an evaporation rate of 0.5～1 Å s^{-1}. The cathode was completed through thermal deposition of LiF at a deposition rate of 0.1 Å s^{-1}, and then capped with Al through thermal deposition at a deposition rate of 3～5 Å s^{-1}. EL luminescence, spectra and CIE color coordinates (1931) were measured with a Spectrascan PR-650 photometer, and the current-voltage characteristics were measured with a computer-controlled Keithley 2400 SourceMeter under ambient atmosphere.

The transient EL decay was tested by an Agilent 8114A pulse generator (100 V/2 A) to generate rectangular pulse voltages. The pulse repetition rate was 1 kHz with the width of 100 μs. The EL signal was detected using a lens coupled with the optical fiber connected to a Hamamatsu photomultiplier (H10721-20) with time resolution of 0.57 ns. The photomultiplier was connected to one of the channels of a digital oscilloscope (Tektronix DPO7104, sampling rate: 5 GS s^{-1}; resolution: 100 μV) with 50 Ω input resistance.

1.4 Computational Detail

The ground-state (S_0) and the lowest singlet excited state (S_1) geometries were optimized at the B3LYP/6-31G(d,p) level, which is a common method to provide molecular geometries and the optimized outcome is in good agreement with the experiment result.

2. Synthesis of Materials

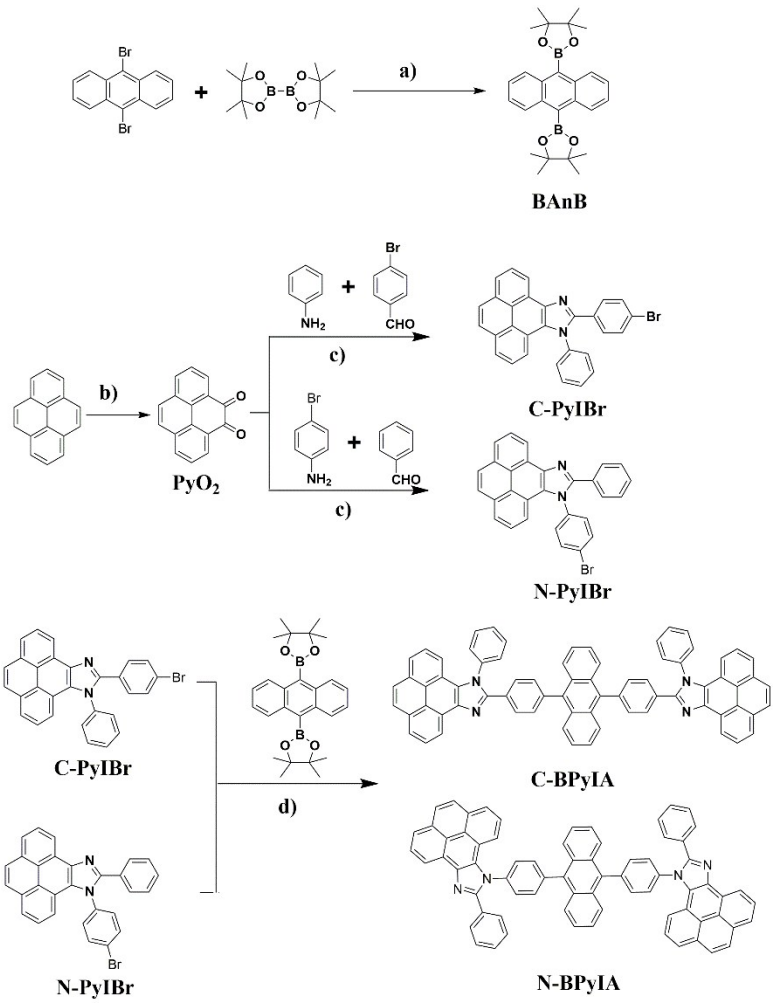

Scheme S1. Synthesis Routes of C-BPyIA and N-BPyIA. a) $Pd(dppf)_2Cl_2$, KOAc, 1,4-dioxane, 85 ℃, N_2 protection, 48 h; b) $NaIO_4$, $RuCl_3$, $CHCl_3$, CH_3CN, overnight; c) CH_3COONH_4, 120 °C, N_2 protection, 2 h; d) Suzuki coupling reaction: $Pd(PPh_3)_4$, K_2CO_3, toluene, 85 °C, 48 h under N_2 protection.

3. Characterization

3.1 Time-of-flight mass spectra

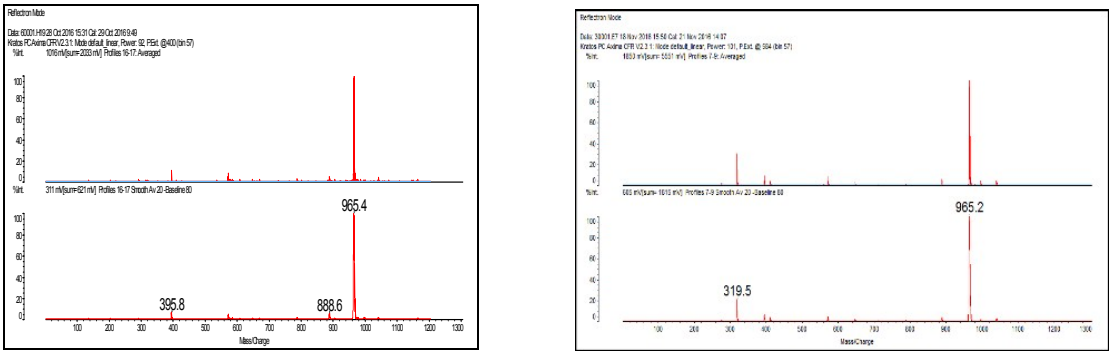

Fig. S1. The time-of-flight mass spectra of C-BPyIA (left) and N-BPyIA (right).

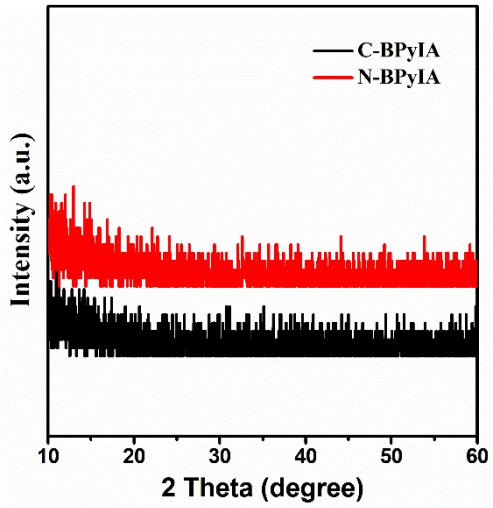

Fig. S2. XRD patterns of C-BPyIA and N-BPyIA in evaporated film.

3.2 Optical Properties

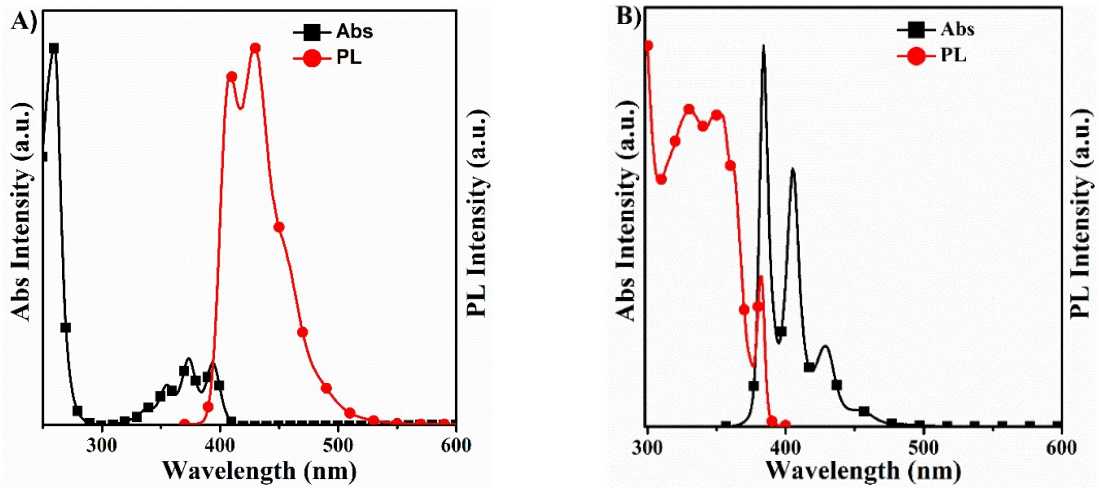

Fig. S3. Absorption and PL spectra of A) PAnP and B) PyI in THF dilute solution.

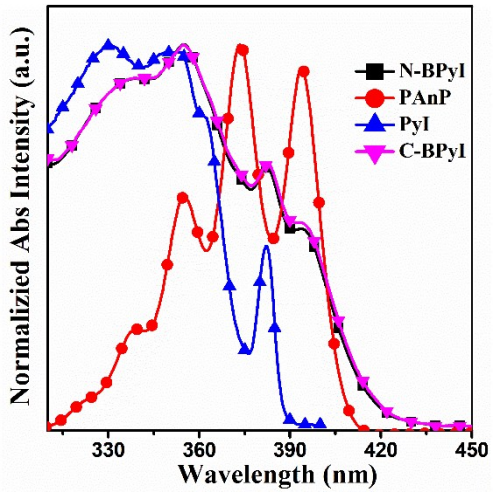

Fig. S4. Absorption spectra of PAnP, PyI, C-BPyIA and N-BPyIA in THF dilute solution.

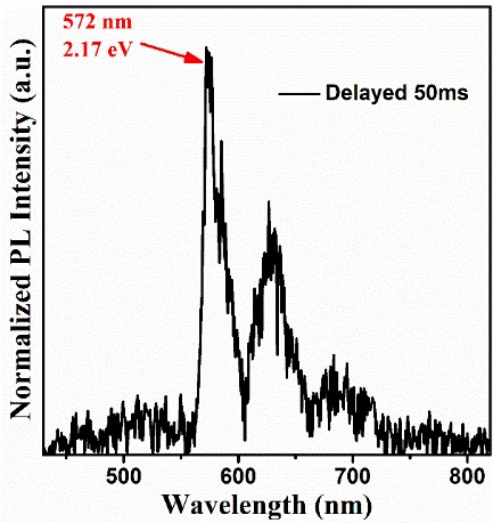

Fig. S5. Phosphorescence of PyI in THF at 78 K.

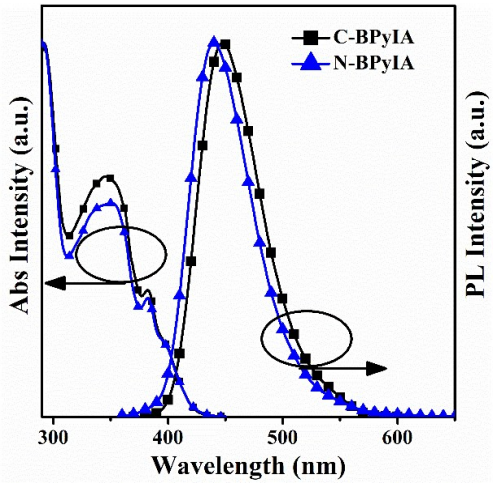

Fig. S6. Absorption and PL spectra of C-BPyIA and N-BPyIA in doped PMMA films (5 wt%).

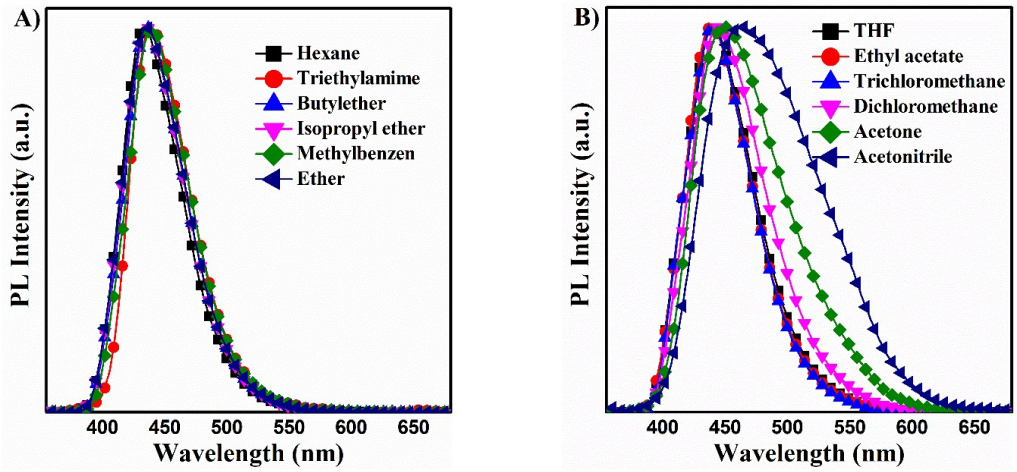

Fig. S7. PL spectra of N-BPyIA in different solvents.

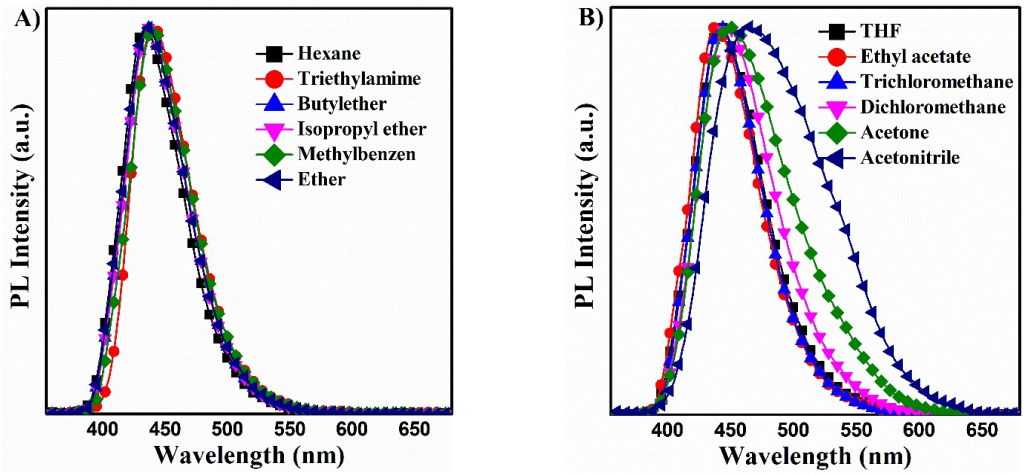

Fig. S8. PL spectra of C-BPyIA in different solvents.

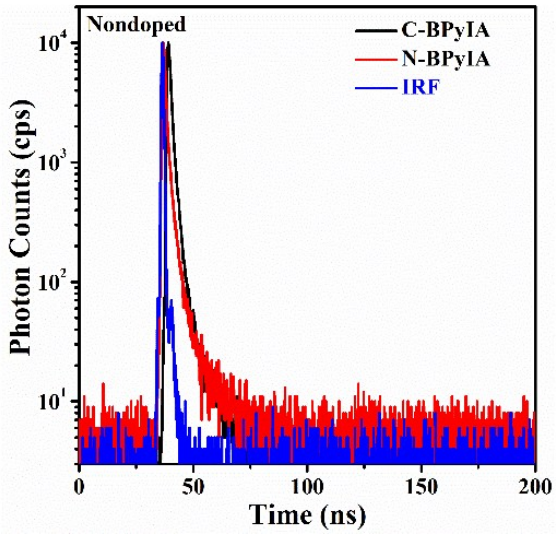

Fig. S9. Fluorescence attenuation curves of C-BPyIA and N-BPyIA in nondoped films.

3.3 Electroluminescence properties of the devices

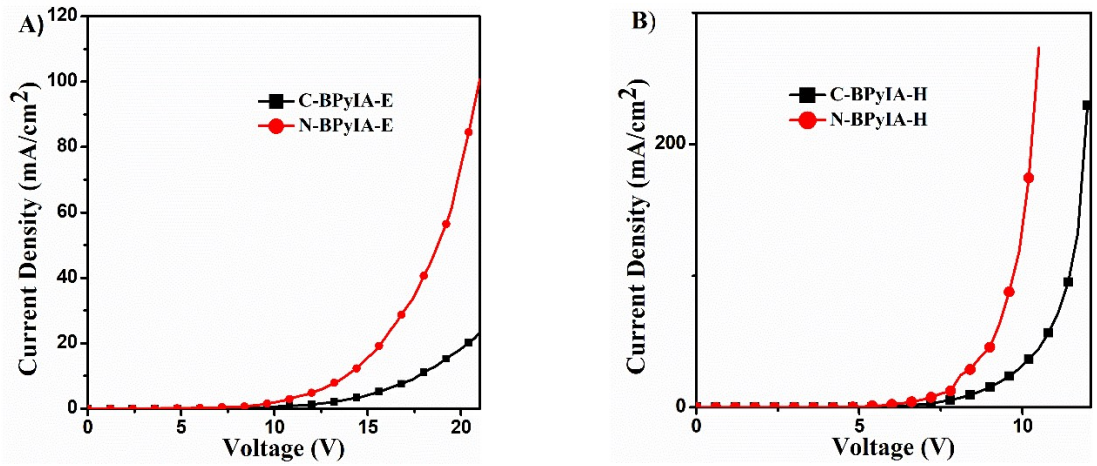

Fig. S10. Current density versus voltage characteristics of the electron-only A) and hole-only devices B) for C-BPyIA and N-BPyIA.

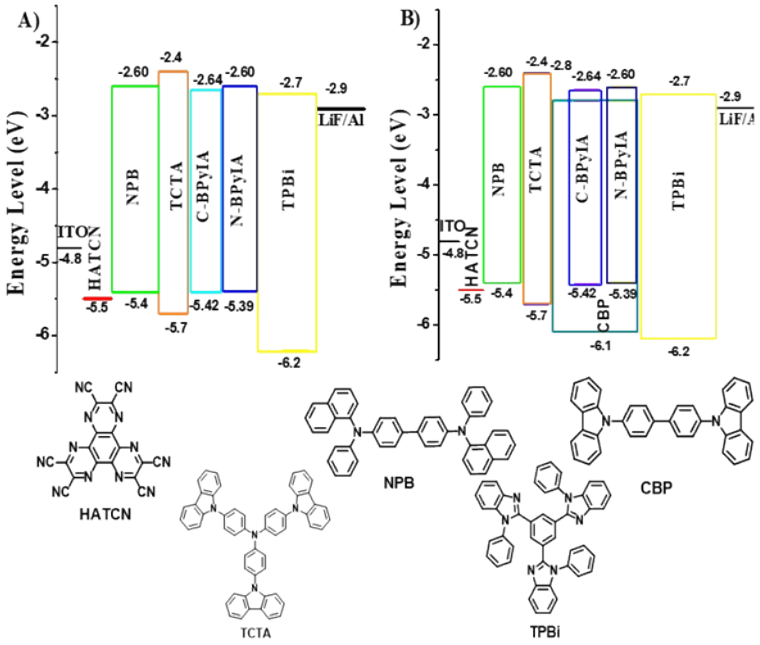

Fig. S11. Energy levels in devices of A) non-doped device, B) doped device as well as the molecular structures of transport materials.

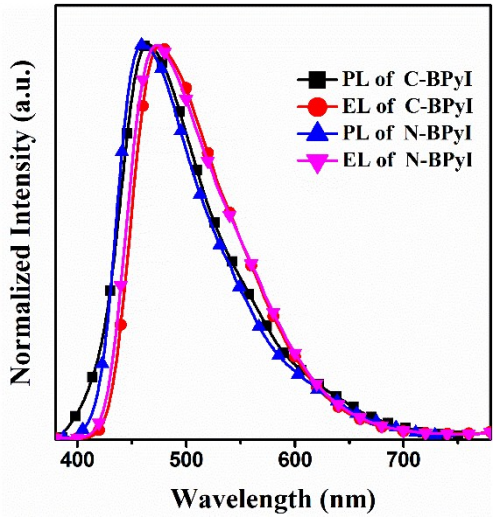

Fig. S12. PL of neat film and EL of the nondoped device for C-BPyIA and N-BPyIA.

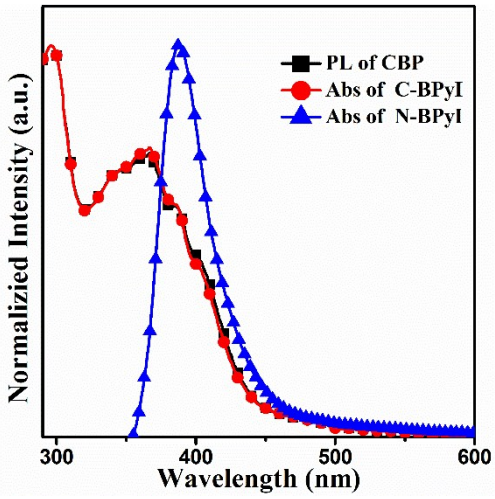

Fig. S13. Absorption of C-BPyIA and N-BPyIA neat film and PL of CBP neat film.

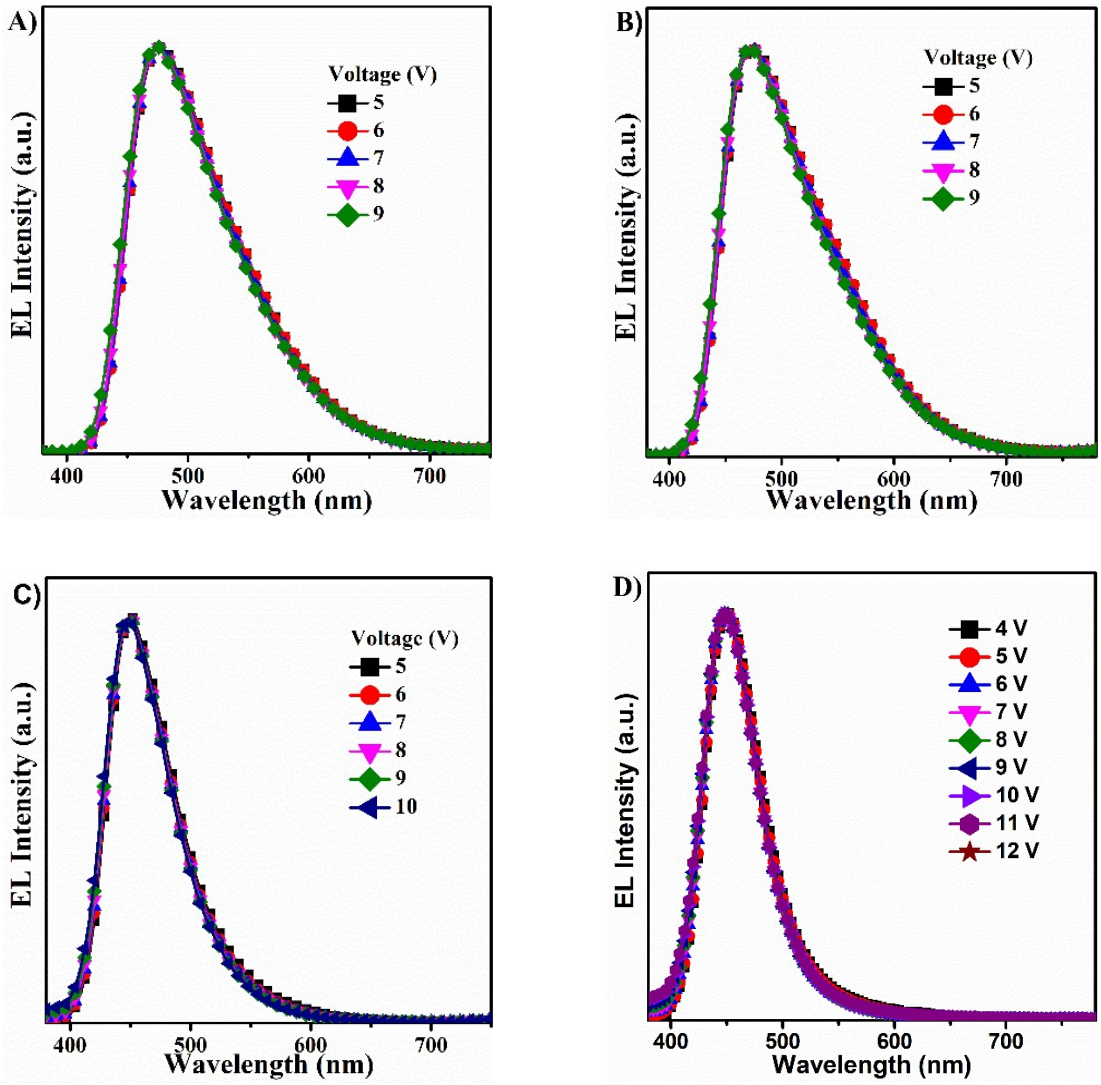

Fig. S14. The EL spectra of non-doped devices A, B and doped devices C, D under the different voltages.

Non-doped devices A, B: ITO/HATCN (6 nm)/TAPC (25 nm)/TCTA (15 nm)/ C-BPyIA or N-BPyIA (20 nm)/TPBi (40 nm)/LiF (1.2 nm)/Al (120 nm);

Doped devices C, D: ITO/HATCN (6 nm)/ TAPC (25 nm)/TCTA (15 nm)/ C-BPyIA or N-BPyIA/CBP-15 wt% (20 nm)/TPBi (40 nm)/LiF (1.2 nm)/Al (120 nm).

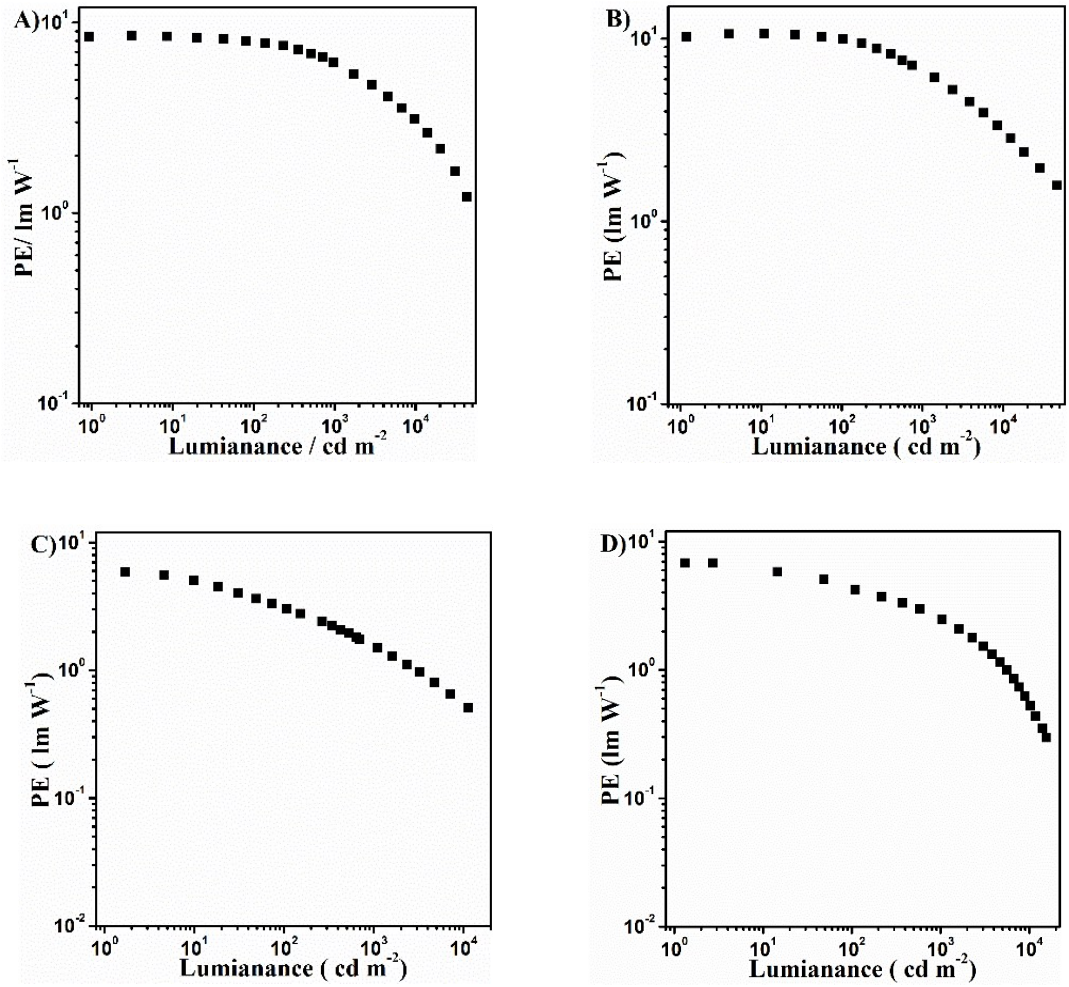

Fig. S15. Power efficiency versus luminance of non-doped devices A, B and doped devices C, D.

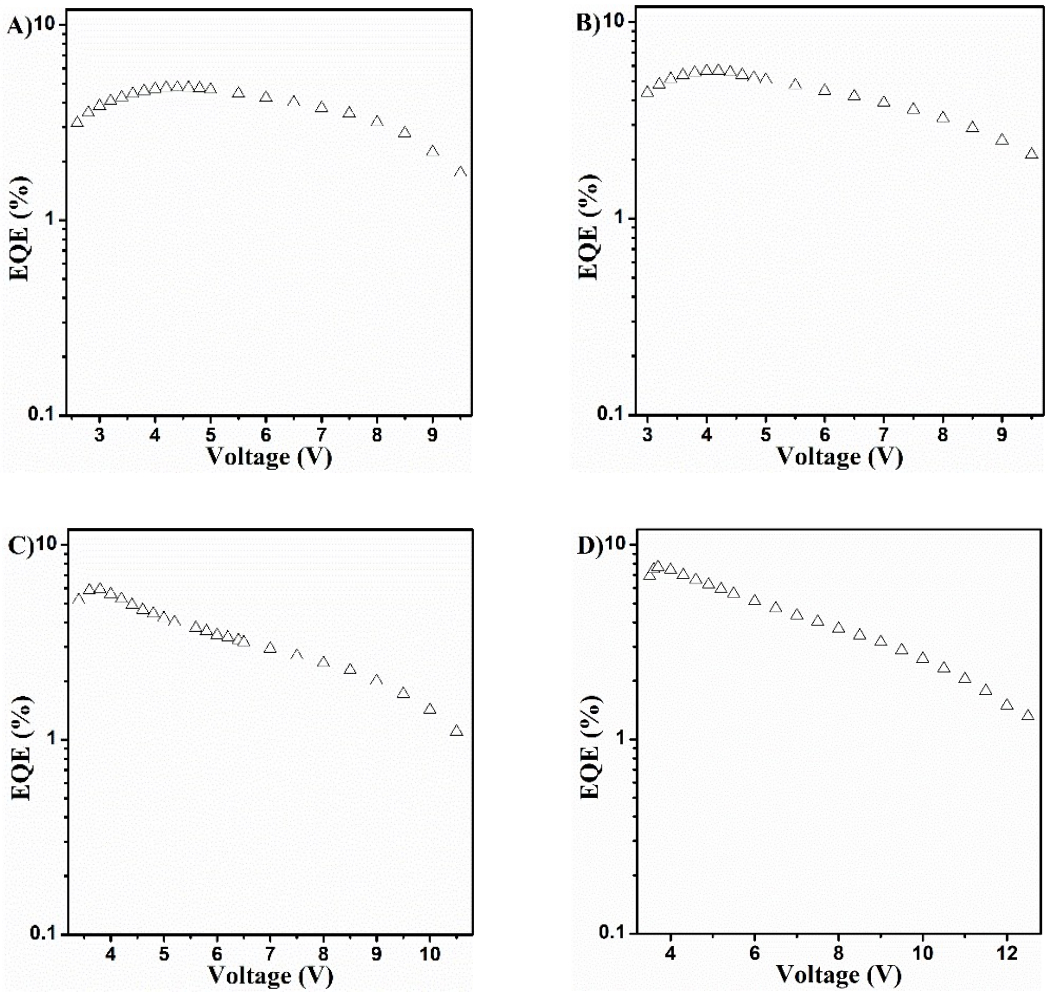

Fig. S16. Voltage dependent EQE of nondoped device A, B and doped device C, D at different voltages.

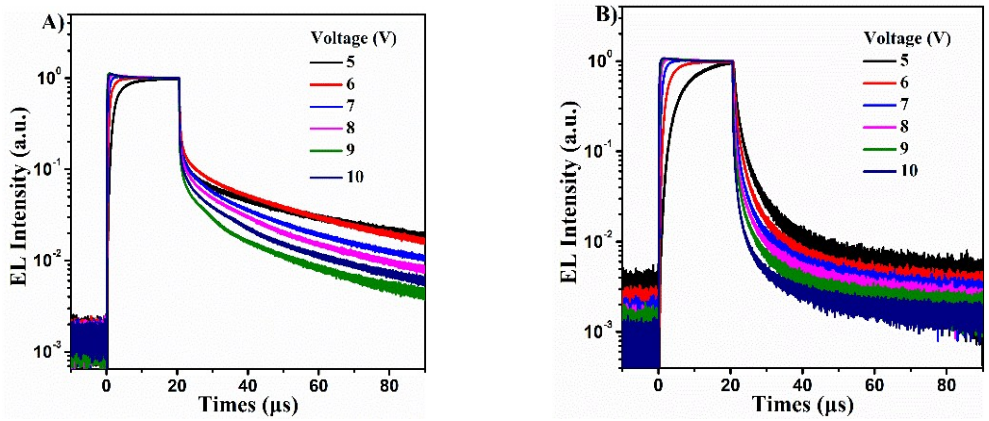

Fig. S17. Transient EL decay of non-doped A) and doped devices B) based on N-BPyIA emitter at different voltages.

Table S1. EL performance of C-BPyIA and N-BPyIA as well as other efficiently blue-emitting materials based An in recent years.

Compound	Structure	Physical Properties				Device Properties				Ref.
		T_d[a]/℃	HOMO/eV	LUMO/eV	φ_{PL}	Host	CE/cd A^{-1}	EQE/%	CIE[e]	
C-BPyIA This work	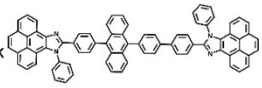	541	-5.42	-2.64	54	CBP	10.12/ 6.69	4.78/ 5.90	(0.21,0.32)/ (0.15,0.12)	
N-BPyIA This work	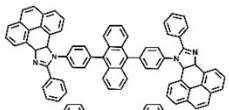	541	-5.41	-5.57	46	CBP	12.64/ 7.98	5.63/ 7.67	(0.22,0.31)/ (0.15,0.10)	
BD3	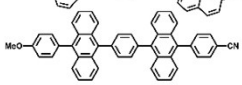	450	-5.52	-2.31	33	CBP	8.2/ 6.1	4.2/ 12	(0.24,0.17)/ (0.15,0.06)	1
3CzAnBzt	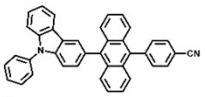	354	-5.59	-2.59	51.3	-	11.72	10.06	(0.14,0.14)	2
DAPBN	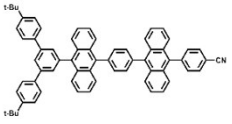	354	-5.53	-2.62	35.2	-	4.46	5.97	(0.15,0.08)	3
pCzAnTAZ	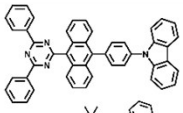	442	-5.64	-2.97	45	-	11.19	5.44	(0.17,0.32)	4
TPE-TADC	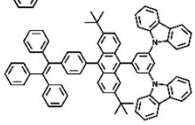	486	-5.37	-2.55	72.8	-	6.81	5.71	(0.16,0.14)	5
TPE-TAPBi	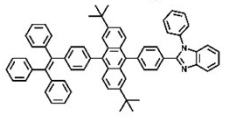	319	-5.41	-2.49	47.8	-	7.21	5.73	(0.15,0.16)	6
PIAnPCN	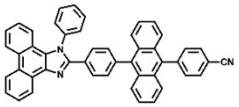	483	-5.55	-2.78	50	CzSi	13.16 /5.95	9.44 /6.77	(0.14,0.19)/ (0.15,0.07)	7
PAC	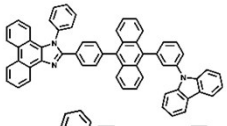	495	-5.54	-2.16	48	-	12.37	10.03	(0.15,0.13)	8
TPA-An-PPI	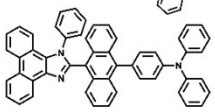	466	-5.25	-2.68	75	-	9.83	4.61	(0.16,0.38)	9
DPA-PIM	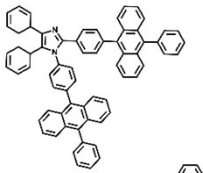	480	-5.58	-2.53	9	-	4.9	6.5	(0.15,0.06)	10
TAT	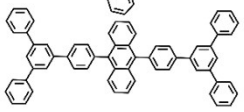	470	-5.54	-5.60	-	-	3.64	7.18	(0.16,0.09)	11
TPAXAN	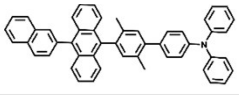	428	-5.59	-2.52	-	-	-	4.62	(0.15,0.05)	12

References

[1] J.-Y. Hu, Y.-J. Pu, F. Satoh, S. Kawata, H. Katagiri, H. Sasabe, J. Kido, *Adv. Funct. Mater.,* 2014, **24**, 2064-2071.

[2] W. Liu, S. Ying, R. Guo, X. Qiao, P. Leng, Q. Zhang, Y. Wang, D. Ma, L. Wang, *J. Mater. Chem. C,* 2019, **7**, 1014-1021.

[3] L. Peng, J.-W. Yao, M. Wang, L.-Y. Wang, X.-L. Huang, X.-F. Wei, D.-G. Ma, Y. Cao, X.-H. Zhu, *Sci. Bull.,* 2019, **64**, 774-781.

[4] W. Liu, S. Ying, Q. Zhang, S. Ye, R. Guo, D. Ma, L. Wang, *Dyes Pig.,* 2018, ***158***, 204-212.

[5] Y. Li, Z. Xu, X. Zhu, B. Chen, Z. Wang, B. Xiao, J. W. Y. Lam, Z. Zhao, D. Ma, B. Z. Tang, *ACS Appl. Mater. Interfaces,* 2019, **11**, 17592-17601.

[6] B. Chen, B. Liu, J. Zeng, H. Nie, Y. Xiong, J. Zou, H. Ning, Z. Wang, Z. Zhao, B. Z. Tang, *Adv. Funct. Mater.,* 2018, **28**, 1803369.

[7] X. Tang, Q. Bai, T. Shan, J. Li, Y. Gao, F. Liu, H. Liu, Q. Peng, B. Yang, F. Li, P. Lu, *Adv. Funct. Mater.,* 2018, **28**, 1705813

[8] Y. Xu, X. Liang, X. Zhou, P. Yuan, J. Zhou, C. Wang, B. Li, D. Hu, X. Qiao, X. Jiang, L. Liu, S. J. Su, D. Ma, Y. Ma, *Adv. Mater.,* 2019, **31**, e1807388.

[9] C. Li, Z. Li, X. Yan, Y. Zhang, Z. Zhang, Y. Wang, *J. Mater. Chem. C,* 2017, **5**, 1973-1980.

[10] C. He, H. Guo, Q. Peng, S. Dong, F. Li, *J. Mater. Chem. C,* 2015, **3**, 9942-9947.

[11] S.-K. Kim, B. Yang, Y. Ma, J.-H. Lee, J.-W. Park, *J. Mater. Chem.,* 2008, **18**, 3376.

[12] R. Kim, S. Lee, K. H. Kim, Y. J. Lee, S. K. Kwon, J. J. Kim, Y. H. Kim, *Chem. Commun.,* 2013, **49**, 4664-4666.